Chinese Journal of Mechanical Engineering

ORIGINAL ARTICLE

Open Access

Analysis and Verification on Buckling Mechanism of Spatial Tow Steering in Automated Fiber Placement

Minghui Yi[1], Fei Liu[1*], Baoning Chang[2], Yingdan Zhu[3], Xilun Ding[1,2] and Wuxiang Zhang[1,2]

Abstract

Automated fiber placement (AFP) enables the efficient and precise fabrication of complex-shaped aerospace composite structures with lightweight and high-performance properties. However, due to the excessive compression on the inner edge of the tow placed along the curved trajectory, the resulting defects represented by buckling and wrinkles in spatial tow steering can induce poor manufacturing accuracy and quality degradation of products. In this paper, a theoretical model of tow buckling based on the first-order shear deformation laminate theory, linear elastic adhesion interface and Hertz compaction contact theory is proposed to analyze the formation mechanism of the wrinkles and predict the formation of defects by solving the critical radius of the trajectory, and finite element analysis involving the cohesive zone modeling (CZM) is innovated to simulate the local buckling state of the steered tow in AFP. Additionally, numerical parametric studies and experimental results indicate that mechanical properties and geometric parameters of the prepreg, the curvature of the placement trajectory and critical process parameters have a significant impact on buckling formation, and optimization of process parameters can achieve effective suppression of placement defects. This research proposes a theoretical modeling method for tow buckling, and conducts in-depth research on defect formation and suppression methods based on finite element simulation and placement experiments.

Keywords Automated fiber placement, Spatial tow steering, Buckling mechanism, Process optimization

1 Introduction

Automated fiber placement (AFP) can realize high-precision forming of laminated composite structures [1–4], such as aeroengine fan blades, aircraft inlets [5], satellite antenna, etc [6]. Nevertheless, unidirectional prepreg tows steered in three-dimensional space by robotic fiber placement can cause defects [7–12] that reduce interlaminar bonding strength, as a result of local compression on the inner edge of the curved tow.

In order to explore the formation mechanism and suppression method of defects in tow steering, Beakou et al. [13] first proposed a local approach for tow buckling modeling of the first ply based on an anisotropic plate on an elastic foundation, and calculated the critical buckling load and steering radius by Ritz energy method [14]. To ameliorate the theoretical model, the deflection function was optimized by Matveev et al. [15] based on more accurate boundary conditions, a tangential shear layer was introduced into the elastic foundation to accurately characterize the shear tackiness, and the stress relaxation function was employed as the description method for time-dependent viscoelastic behavior of the interfacial tackiness.

*Correspondence:
Fei Liu
feiliulf@buaa.edu.cn
[1] School of Mechanical Engineering and Automation, Beihang University, Beijing 100191, China
[2] Advanced Manufacturing Center, Ningbo Institute of Technology, Beihang University, Ningbo 315100, China
[3] Ningbo Institute of Materials Technology and Engineering, Chinese Academy of Sciences, Ningbo 315201, China

Kheradpisheh and Hojjati [16] adopted Koiter imperfection model to modify the deflection through the amplitude evolution process of the wrinkles, and solved the critical value employing Galerkin method and the finite difference method (FDM). However, according to Belhaj's research, the prepreg tackiness plays an important role in inhibiting the formation of defects, and the linear elastic layer employed above cannot accurately characterize the interfacial performance [17]. A global modeling approach [18] was proposed by Nima to capture the trends, patterns, and frequency of wrinkles and blisters, of which the main strategy is to simulate the prepreg tack through Cohesive Zone Modeling (CZM). An optimized local theoretical model based on contact mechanics was combined with the global simulation analysis to elaborate the defects formation mechanism, and the models were verified by sufficient trials qualitatively with the influence of process parameters.

The aforementioned researches on buckling models focus on the influence of lateral bending of local prepreg tow on the formation of wrinkles in two-dimensional plane [19–21], limiting the application of theoretical analysis methods in tow steering tremendously. The placement trajectory of aerospace structures based on AFP possesses high complexity and multiple characteristics [22], limited by the complex geometric features and bearing conditions, which is manifested in a complicated bending-torsion coupling state in three-dimensional space, including the horizontal bending along the width direction of the prepreg in placement surface and the rotation of the cross-section in space. The simple plane deformation theory of lateral bending cannot meet the analysis requirements of spatial tow steering for heterotypic structure, and the modeling strategy and characterization method for buckling and wrinkles in spatial tow steering is still in blank. In addition, there is a necessity to analyse the influence of the contact state [23–26] between the compaction roller and the tows in depth to reveal the causes for defects formation, and the theoretical model can be modified and ameliorated to be in quite good agreement with the actual conditions.

In this paper, a theoretical model with solution procedures of tow buckling in spatial tow steering based on the first-order shear deformation laminate theory is established for complex structure forming, and an approach for simulation modeling and numerical analysis is established to reveal the influence of the coefficients in theoretical model. Sufficient AFP experiments to validate the buckling theory have been conducted and the results are illustrated in detail to demonstrate the inhibitory effect of optimized processes on defects. Finally, the achievements are summarized compendiously with deficiencies at present for further research on defect suppression in spatial tow steering, in order to improve the forming quality of composite structures.

2 Modeling Approach for Tow Buckling

Considering that the research objective of this paper is the mechanism and prediction method of tow buckling under the bending-torsion coupling state in three-dimensional space, which is being laid on the layers or the mold, it is necessary to develop the tow steering model on laminates with complex surfaces. The buckling of the spatial steered tow proposed in this section can be modelled as the out-of-plane wrinkles [27] of a rectangular plate placed on an elastic foundation under non-uniform bending-torsional coupling loads. Among them, the elastic foundation is used to indicate the degree of adhesion between the tows to be laid and the layers or the mold, and the external loads are applied through the cooperation of the compaction roller and the mold with complex surface.

2.1 Adhesion Characterization Method

In the process of progressive placement, the resin flows and fuses at the interface between the layers and the tow to be laid under compaction and heating, resulting in a certain degree of interlayer bonding [28]. Due to the fact that the time-varying stress-strain relationship of the resin matrix is not a research focus, the Pasternak linear elastic foundation [29] is used to establish the theoretical model of interfacial stress caused by tow buckling. The elastic interfacial model established is illustrated in Figure 1. The elastic properties of the interlaminar adhesion are simulated by spring elements. Wherein, the stiffness coefficient k of the spring can be used to characterize the relationship between the separation interfacial stress and the peeling displacement.

In this paper, the adhesion of the prepreg [30–33] is characterized as an elastic interface composed of elastic elements, which can be mathematically expressed as:

$$q(x,y) = k\omega(x,y), \tag{1}$$

where q is the adhesive stress between the tow and the layers or the mold, k is the stiffness coefficient of the adhesion interface, and ω is the displacement of the tow along its surface normal direction, which will be denoted by the deflection hereinafter.

2.2 Spatial Tow Steering Theory

Different from the traditional lateral bending buckling model of plate structure based on classical laminate theory, the prepreg tows for the placement of complex structures are usually in the bending-torsion coupling state, and the 2D model neglecting the normal

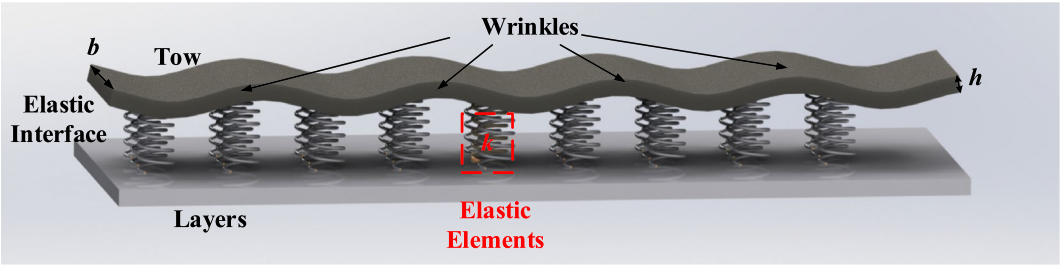

Figure 1 Diagram of the interfacial model based on elastic foundation

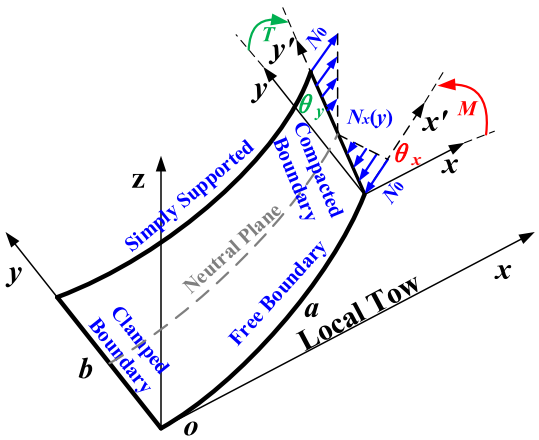

Figure 2 Schematic diagram of tow spatial deformation

shear deformation cannot accurately describe the complex deformation state of the steered tow. In this paper, the three-dimensional deformation state of the tows is decomposed into the rotation of the cross-section around the Cartesian coordinate axes, where the rotation around the z-axis is used to reflect the in-plane bending of the tow under the compression and rotational traction of the compaction roller, while the rotation around the x-axis and y-axis is attributed to the constraints of the geometric characteristics of the mold surface.

2.2.1 3-D Deformation Theoretical Model

In order to establish the steered tow deformation model consistent with the actual working conditions, based on the local analysis method, the following assumptions are made:

(1) As shown in Figure 2, the four edges of the local tow to be analyzed are in different states of stress and deformation. The two edges along the width direction of the tow are fixed, that is, the initial boundary and the compacted boundary do not buckle, while the compressed inner side is free to form buckling and wrinkles, and the tensile edge is a simply supported boundary with good adhesion to the mold.

(2) The cross-section of the tow is subjected to coupling in-plane bending moment longitudinal spatial torque T and out-of-plane bending moment M under the interaction between compaction roller and mold, which results in local transverse bending, three-dimensional torsion and warpage of the tow, respectively. The in-plane bending moment is represented by linear loads symmetrical to the neutral plane, while the spatial torsions are characterized by the rotation angle θ_x and θ_y of the tow section.

Different from Kirchhoff thin plate hypothesis [34], the normal shear deformation is introduced into the tow steering model to represent the complex deformation state of the prepreg in spatial steering, and then the spatial buckling model for the placement of complicated parts can be constructed and analyzed.

Based on the first-order shear deformation laminate theory, the torsion angle of the tow cross-section around the x-axis is θ_y, and the warpage angle around the y-axis is θ_x, so the displacement field of the local tow in spatial steering can be expressed as

$$\begin{cases} u(x,y,z) = u_0(x,y) - z\omega_{,x} + z\theta_x(x,y), \\ v(x,y,z) = v_0(x,y) - z\omega_{,y} + z\theta_y(x,y), \\ \omega(x,y,z) = \omega(x,y), \end{cases} \tag{2}$$

where u is the displacement along the x-axis direction, v is the displacement along the y-axis direction, and the subscript comma represents the derivation of the physical quantity.

The introduction of rotation angles around the coordinate axes achieves the characterization of the deformation of fiber tows in three-dimensional space, which enables the tow buckling theory to break through the limitations of two-dimensional planes and expands the application to complex structures.

Then, the strain-displacement equation can be expressed as

$$\begin{cases} \boldsymbol{\varepsilon} = \begin{bmatrix} \varepsilon_x \\ \varepsilon_y \\ \gamma_{xy} \end{bmatrix} = \begin{bmatrix} -z\omega_{,xx} + z\theta_{x,x} \\ -z\omega_{,yy} + z\theta_{y,y} \\ z\theta_{x,y} + z\theta_{y,x} - 2z\omega_{,xy} \end{bmatrix}, \\ \boldsymbol{\gamma} = \begin{bmatrix} \gamma_{xz} \\ \gamma_{yz} \end{bmatrix} = \begin{bmatrix} \theta_x \\ \theta_y \end{bmatrix}, \end{cases} \tag{3}$$

where ε is the normal strain of the local tow, and the γ is the shear strain.

The stress-strain relationship can be obtained as

$$\begin{cases} \boldsymbol{\sigma} = \begin{bmatrix} \sigma_x \\ \sigma_y \\ \tau_{xy} \end{bmatrix} = Q_1\boldsymbol{\varepsilon} = \begin{bmatrix} Q_{11} & Q_{12} & 0 \\ Q_{12} & Q_{22} & 0 \\ 0 & 0 & Q_{66} \end{bmatrix} \begin{bmatrix} \varepsilon_x \\ \varepsilon_y \\ \gamma_{xy} \end{bmatrix}, \\ \boldsymbol{\tau} = \begin{bmatrix} \tau_{xz} \\ \tau_{yz} \end{bmatrix} = Q_2\boldsymbol{\gamma} = \begin{bmatrix} Q_{55} & 0 \\ 0 & Q_{44} \end{bmatrix} \begin{bmatrix} \gamma_{xz} \\ \gamma_{yz} \end{bmatrix}, \end{cases} \tag{4}$$

where σ is the normal stress of the tow, τ is the shear stress, and $\boldsymbol{Q}$ is the simplified stiffness matrix:

$$\begin{cases} Q_{11} = \dfrac{E_{11}}{1 - \nu_{12}\nu_{21}}, \\ Q_{12} = \dfrac{\nu_{12}E_{22}}{1 - \nu_{12}\nu_{21}}, \\ Q_{22} = \dfrac{E_{22}}{1 - \nu_{12}\nu_{21}}, \\ Q_{44} = G_{23}, \\ Q_{55} = G_{13}, \\ Q_{66} = G_{12}, \end{cases} \tag{5}$$

where E is the tensile modulus of the tow, ν is the Poisson's ratio, and G is the shear modulus.

Continuous fiber prepreg is orthotropic, therefore the stiffness coefficient matrix $\boldsymbol{Q}$ is a symmetric matrix. Due to the negligible variation of deflection along the thickness direction, the values of the elements Q_{13} and Q_{23} are 0.

2.2.2 Boundary Conditions and Mechanical Analysis

On the basis of actual placement trials, we assume that the initial edge of the local tow cannot buckle or rotate relative to the mold, and the research object focuses on the edge compacted under the roller to describe its state in three-dimensional space, thus characterizing the tow spatial steering.

The tow in the initial placement region is laid horizontally and straight, of which the deflection, rotation angles and their variation trend are all zero, resulting in a fixed initial edge. The edge being compacted is stationary relative to the mold in normal direction, that is, there is no buckling deflection or tendency. The rotation angle of the compacted edge around the x-axis, defined as torsion angle, varies continuously along the length of the tow and gradually increases from zero to a specific value, and remains constant along the width due to the narrow width of the prepreg. Simultaneously, in order to refine the model, this paper stipulates that the rotation angle of the compacted edge around the y-axis, i.e. the warpage angle, changes along the x-axis, that is, the tow is laid horizontally at the beginning, and the placement trajectory gradually rotates around the y-axis as the laying length increases, while the angle keeps invariant across the width.

The compacted edge is steered to bend laterally due to the moment generated by the rotation of the compaction roller tangent to the mold surface, resulting in the compression on the inner side and the extension on the outer side of the tow. When the compressive load exceeds the critical value, buckling instability occurs on the compressed edge in spite of the adhesion between the tow and the mold, manifested as the formation of wrinkles. Furthermore, torsion of the tow around the x-axis and warpage around the y-axis also affect the formation of defects.

On these grounds, the kinematic boundary conditions of the three-dimensional deformation model of the steered tow are as

$$\begin{cases} \omega(x=0) = 0,\ \omega_{,x}(x=0) = 0, \\ \omega(x=a) = 0,\ \omega_{,x}(x=a) = 0, \\ \omega\big(y=b\big) = 0,\ \omega_{,yy}\big(y=b\big) = 0, \\ \theta_y(x=0) = 0,\ \theta_{y,x}(x=0) = 0, \\ \theta_x(x=0) = 0,\ \theta_{x,x}(x=0) = 0, \end{cases} \tag{6}$$

where a is the length of the local tow, and b is the width.

The in-plane bending moment of the tow cross-section can be simplified as loads distributed linearly and symmetrically along the width, thus a free-stress neutral plane is formed at the center of the local tow, as shown in Figure 2. The external loads along the y-axis distributed in the cross-section of the tow can be supposed as

$$N_x\big(y\big) = \frac{2N_0}{b}y - N_0, \tag{7}$$

where N_0 is the maximum value of the in-plane load, located at the boundary of the cross-section of the prepreg tow.

In addition to the in-plane linear loads, the external forces also comprise the torque and moment applied to the tow by the compaction roller and mold that cause distortion and warping deformation, and the effect of external force work on the buckling model will be elucidated below.

2.2.3 Improved Solution Procedure

In the first step, an improved deflection equation for tow buckling is proposed, which satisfies the boundary conditions completely and accurately.

$$\omega(x,y)=\sum_{m=1}^{\infty}\sum_{n=1}^{\infty}\omega_{mn}\left(1-\cos\frac{2m\pi x}{a}\right)\cos\frac{(2n-1)\pi y}{2b}, \tag{8}$$

where ω_{mn} is the undetermined deflection coefficient.

The angle equations for the rotation of the tow cross-section around the x-axis and y-axis are

$$\begin{cases}\theta_y(x)=\sum_{m=1}^{\infty}\theta_m\left(1-\cos\frac{(2m-1)\pi x}{2a}\right),\\ \theta_x(x)=\sum_{n=1}^{\infty}\theta_n\left(1-\cos\frac{(2n-1)\pi x}{2a}\right),\end{cases} \tag{9}$$

where θ_m and θ_n are the coefficients of the angles.

The rotation angle equations established above satisfy the torsional boundary conditions, and can be used to characterize the force and deformation state of the local tows in spatial steering for the formation of complex structures.

It can be concluded from Eq. (9) that the angles vary along the x-axis, which can be assumed to be constant across the y-axis direction due to the narrow width of the prepreg tow.

Secondly, the in-plane strain potential energy equation of the tow can be obtained as

$$U=\frac{1}{2}\int_0^a\int_0^b\begin{bmatrix}D_{11}\left(\theta_{x,x}-\omega_{,xx}\right)^2+2D_{12}\left(\theta_{y,y}-\omega_{,yy}\right)\\ \left(\theta_{x,x}-\omega_{,xx}\right)+D_{22}\left(\theta_{y,y}-\omega_{,yy}\right)^2+\\ D_{66}\left(\theta_{x,y}+\theta_{y,x}-2\omega_{,xy}\right)^2+A_{55}\theta_x^2+A_{44}\theta_y^2\end{bmatrix}\mathrm{d}x\mathrm{d}y, \tag{10}$$

with

$$\begin{cases}A_{ij}=\int_0^h Q_{ij}\mathrm{d}z=Q_{ij}h,\\ D_{ij}=\int_0^h Q_{ij}z^2\mathrm{d}z=\frac{1}{3}Q_{ij}h^3,\end{cases} \tag{11}$$

where h is the thickness of the prepreg, A is tensile stiffness matrix, and D is bending stiffness matrix.

Subsequently, the potential energy of the elastic interface is given by

$$\begin{aligned}V&=\frac{1}{2}\int_0^a\int_0^b q(x,y)\omega(x,y)\mathrm{d}x\mathrm{d}y\\&=\frac{1}{2}\int_0^a\int_0^b k\omega^2\mathrm{d}x\mathrm{d}y.\end{aligned} \tag{12}$$

The work done by the in-plane loads on the local tow can be expressed as

$$\begin{aligned}W_1&=\frac{1}{2}\int_0^a\int_0^b N_x\omega_{,x}^2\mathrm{d}x\mathrm{d}y\\&=\frac{1}{2}\int_0^a\int_0^b\left(\frac{2N_0}{b}y-N_0\right)\omega_{,x}^2\,\mathrm{d}x\mathrm{d}y.\end{aligned} \tag{13}$$

The work done by the cross-sectional torque of the tow is written as

$$\begin{aligned}W_2&=\frac{1}{2}\int_0^a\int_0^b\frac{T\theta_y}{x^2}\mathrm{d}x\mathrm{d}y\\&=\frac{1}{2}\int_0^a\int_0^b G_{12}\beta bh^3\frac{\theta_y^2}{x^3}\mathrm{d}x\mathrm{d}y\approx\frac{1}{2}\theta_m^2\frac{G_{12}\beta bh^3}{a},\end{aligned} \tag{14}$$

where the coefficient β can be taken as 0.32.

And the work done by the out-of-plane bending moment can be simplified as

$$W_3=\frac{1}{2}\int_0^a\int_0^b\frac{M\theta_x}{x^2}\mathrm{d}x\mathrm{d}y\approx\frac{1}{2}\theta_n^2\frac{E_{11}bh^3}{12a}. \tag{15}$$

According to the Rayleigh-Ritz method, the total potential energy of the buckling model system can be presented in the form

$$\Pi=U+V-|W_1+W_2+W_3|. \tag{16}$$

By substituting Eqs. (9), (11)-(14) into Eq. (15), the total energy equation can be extended as follows

$$\Pi=\frac{1}{2}\sum_{m=1}^{\infty}\sum_{n=1}^{\infty}\begin{bmatrix}D_{11}E_{mn}+2D_{12}F_{mn}+D_{22}G_{mn}+\\ D_{66}H_{mn}+A_{55}I_{mn}+A_{44}J_{mn}+\\ \frac{3}{4}abk\omega_{mn}^2-\omega_{mn}^2\frac{m^2}{(2n-1)^2}\frac{2bN_0}{a}\\ -\theta_m^2\frac{G\beta bh^3}{a}-\theta_n^2\frac{E_{11}bh^3}{12a}\end{bmatrix}, \tag{17}$$

with

$$
\begin{cases}
E_{mn} = \left[\begin{array}{l} \theta_n^2 \dfrac{(2n-1)^2\pi^2 b}{8a} + \omega_{mn}^2 \dfrac{2m^4\pi^4 b}{a^3} + \\ (-1)^n \omega_{mn}\theta_n \dfrac{16m^2 b}{a^2}\left(\dfrac{1}{4m+2n-1} + \dfrac{1}{2n-1-4m}\right) \end{array}\right], \\
F_{mn} = \left[\begin{array}{l} \omega_{mn}^2 \dfrac{m^2(2n-1)^2\pi^4}{8ab} + (-1)^{n+1}\omega_{mn}\theta_n \\ \dfrac{(2n-1)^2}{2b}\left(\dfrac{2}{(2n-1)} - \dfrac{1}{4m+2n-1} - \dfrac{1}{2n-1-4m}\right) \end{array}\right], \\
G_{mn} = \omega_{mn}^2 \dfrac{3(2n-1)^4\pi^4 a}{128b^3}, \\
H_{mn} = \left[\begin{array}{l} \theta_m^2 \dfrac{(2m-1)^2\pi^2 b}{8a} + \omega_{mn}^2 \dfrac{m^2(2n-1)^2\pi^4}{2ab} + \\ (-1)^m \omega_{mn}\theta_m \dfrac{8m(2m-1)}{a}\left(\dfrac{1}{6m-1} + \dfrac{1}{2m+1}\right) \end{array}\right], \\
I_{mn} = \theta_n^2\left[\dfrac{3a}{2} + (-1)^n \dfrac{4a}{(2n-1)\pi}\right]b, \\
J_{mn} = \theta_m^2\left[\dfrac{3a}{2} + (-1)^m \dfrac{4a}{(2m-1)\pi}\right]b.
\end{cases} \tag{18}
$$

In order to achieve an efficient prediction of defect formation, it is necessary to solve the critical load N_{cr} for buckling, and only the critical value for the first buckling mode will be deduced in this paper, i.e. m and n are taken as 1. Based on the principle of minimum potential energy, differentiation of total potential energy with respect to deflection coefficient and maximum angles leads to the relationship between deflection coefficient, rotation angles and critical load of the tow in steady state:

$$
\frac{\partial \prod}{\partial \theta_m} = \frac{\partial \prod}{\partial \theta_n} = \frac{\partial \prod}{\partial \omega_{mn}} = 0. \tag{19}
$$

Furthermore, the critical in-plane load and trajectory radius for tow buckling can be derived as

$$
\begin{aligned}
N_{cr} = {} & D_{11}\left[\frac{\pi^4}{a^2} + \frac{\theta_n}{\omega_{mn}}\frac{8}{15a}\right] + D_{12}\left[\frac{\pi^4}{8b^2} + \frac{\theta_n}{\omega_{mn}}\frac{8a}{15b^2}\right] \\
& + D_{22}\frac{3\pi^4 a^2}{256b^4} + D_{66}\left[\frac{\pi^4}{4b^2} - \frac{\theta_m}{\omega_{mn}}\frac{16}{15b}\right] + \frac{3}{8}a^2,
\end{aligned} \tag{20}
$$

with

$$
\begin{cases}
\dfrac{\theta_n}{\omega_{mn}} = -\dfrac{D_{11}\frac{32b}{15a^2} + D_{12}\frac{32}{15b}}{D_{11}\frac{\pi^2 b}{4a} + A_{55}\left(3a - \frac{8a}{\pi}\right)b - \frac{E_{11}bh^3}{6a}}, \\
\dfrac{\theta_m}{\omega_{mn}} = \dfrac{D_{66}\frac{64}{15a}}{D_{66}\frac{\pi^2 b}{4a} + A_{44}\left(3a - \frac{8a}{\pi}\right)b - \frac{2G\beta bh^3}{a}}.
\end{cases} \tag{21}
$$

According to the moment-curvature relationship, the critical radius for fiber bundle buckling can be obtained:

$$
R_{cr} = \frac{E_{11}bh}{2N_{cr}}, \tag{22}
$$

where R_{cr} is the critical radius of the steered tow.

2.3 Refinement Method for Buckling Mechanism

It can be seen from Eq. (20) that the adhesion coefficient of the elastic interface k needs to be determined, which is closely related to the interlaminar bonding performance and placement forming quality. In addition, the lack of correlation between the theoretical model for spatial steering and the placement technique will not be conducive to the comprehensive optimization of process parameters, resulting in great importance of the identification of the adhesion coefficients and introduction of process parameters into the buckling model in this section.

2.3.1 Identification of Adhesion Coefficient

The adhesion coefficient k can be used to characterize the relationship between the peeling force and detaching displacement [35], which can be regarded as a linear function based on previous peeling tests. Therefore, k is the time-independent slope of the force-displacement curve before the tow completely separates from the mold.

The intimate contact theory [36] is used to represent the actual contact degree between the bonded layers to

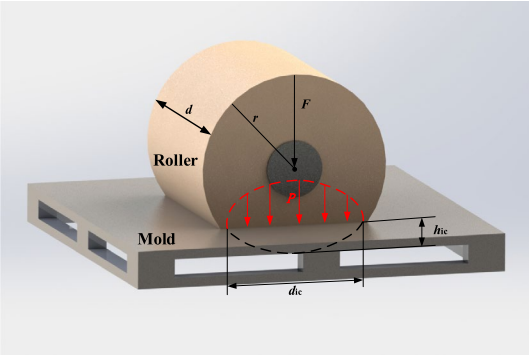

Figure 3 Schematic diagram of the circular cantilever beam

characterize the adhesion coefficient k in this paper, of which the expression is

$$k = \alpha\left(\frac{P}{\eta}t_{ic}\right)^{1/5} = \alpha\left(\frac{Pd_{ic}}{\eta V}\right)^{1/5}, \tag{23}$$

where α is the coefficient related to the geometric morphology of the initial prepreg surface, P is the compaction pressure exerted by the roller on the tow, t_{ic} is the contact time between the tow and the roller, η is the temperature-dependent viscosity of the resin matrix, d_{ic} is the width of contact area, and V is the placement velocity.

The viscosity η of the resin can be obtained by the empirical relationship between liquid viscosity and temperature:

$$\eta = Ae^{\frac{B}{K}}, \tag{24}$$

where A and B are empirical constants, and K is the thermodynamic temperature.

2.3.2 Compaction Pressure Distribution

The flexible roller will deform to a certain extent during the compaction process, resulting in a direct effect on the magnitude and distribution of the pressure decided by the compaction force and roller material [37]. The distribution of compaction pressure can be divided into longitudinal distribution along the length direction of the tow and transverse distribution along the width in the real-time contact area. Due to the narrow width of the prepreg, the transverse distribution of pressure is considered to be uniform, while the longitudinal distribution induces the maximum pressure.

A placement compaction theory of pressure distribution based on Hertz theory can be proposed, in which the contact between the flexible roller and the mold can be regarded as the contact between an elastic cylinder and rigid semi-infinite body, as shown in Figure 3. Wherein, r is the radius of the compaction roller, h_{ic} is the deformation depth, and d is the width of the roller.

Based on Hertz contact theory, the deformation depth is linearly proportional to the compaction force:

$$h_{ic} = \frac{4F}{\pi E^* d}, \tag{25}$$

where $E^* = \frac{E}{1-v_r^2}$, E is the elastic modulus of the roller, v_r is Poisson's ratio, and F is the compaction force.

The width of the contact area can be given by

$$d_{ic} = 2\sqrt{rh_{ic}} = 4\sqrt{\frac{Fr}{\pi dE^*}}. \tag{26}$$

Then, the compaction pressure is calculated by

$$P = \frac{E^* h_{ic}}{d_{ic}} = \sqrt{\frac{FE^*}{\pi rd}}. \tag{27}$$

Substituting Eqs. (26) and (27) into Eq. (23), a new expression of the adhesion coefficient k can be reorganized as

$$k = \alpha\left(\frac{4F}{\pi\eta \mathrm{d}V}\right)^{1/5}. \tag{28}$$

3 Numerical Analysis and Simulation

In order to reveal the relationship between the model parameters and the critical radius of placement trajectory, the effects of material properties and process

Table 1 Material properties and model parameters

Parameters	E_{11}**(MPa)**	E_{22}**(MPa)**	G_{12}**(MPa)**	G_{23}**(MPa)**
Values	121000	8600	4700	3100
Parameters	G_{13}**(MPa)**	v_{12}	v_{21}	h**(mm)**
Values	4700	0.27	0.0192	0.15
Parameters	r**(mm)**	d**(mm)**	E **(MPa)**	v_r
Values	20	30	7.845	0.48

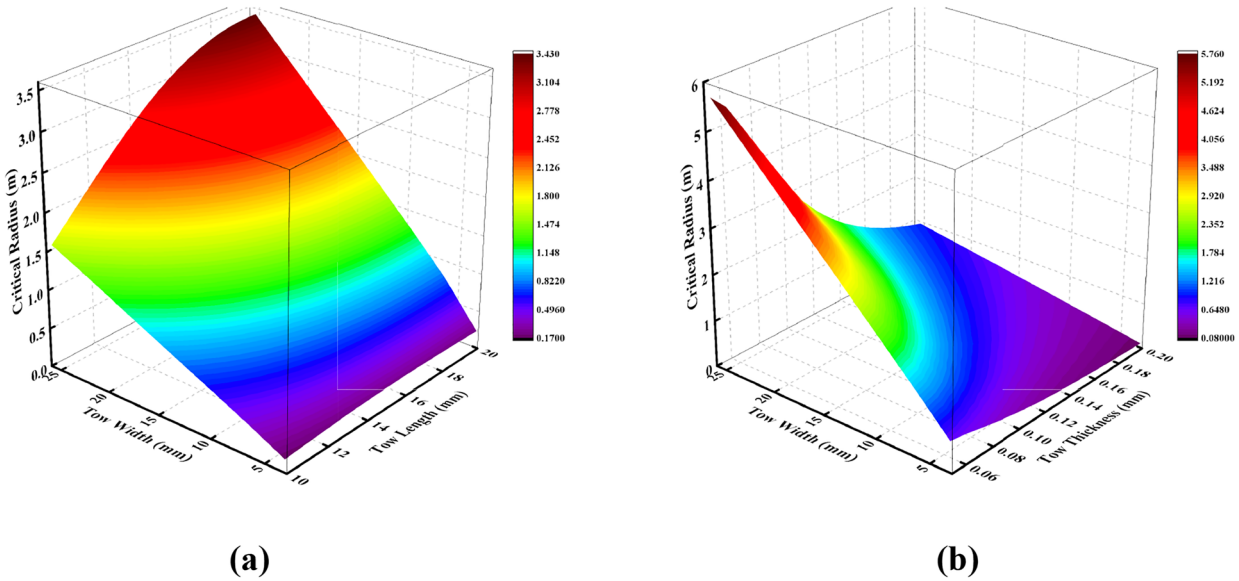

Figure 4 Effect of prepreg parameters: **a** Effect of tow length with different widths, and (**b**) Effect of tow thickness with different widths

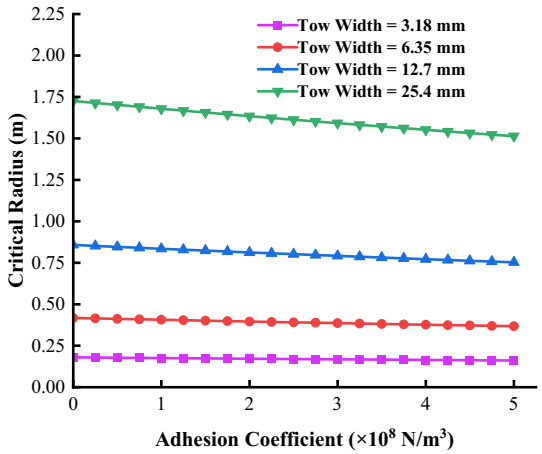

Figure 5 Effect of the adhesion coefficient

conditions are analysed in detail. Furthermore, the finite element software is employed to establish the simulation model of forming defects for qualitative validation.

3.1 Influence of Theoretical Model Coefficients

Based on the experimental data and measurements, the material properties and device parameters used in the theoretical model are shown in Table 1. In addition, the adhesion coefficient of the bonding interface is assumed to be 2.25×10^8 N/m^3.

3.1.1 Effect of the Prepreg Parameters

It can be concluded from Eq. (20) that the geometric parameters of the prepreg material have a significant influence on the critical in-plane load for the buckling of the spatial steered tow, including the length, width and thickness of the prepreg. The effects of prepreg parameters are investigated and analyzed in detail below, and four common widths of tows were selected for comparison.

Figure 4a shows the critical radii for tow buckling at different lengths and widths. For tows with different widths, the longer the length, the larger the critical trajectory radius for buckling, i.e. the more prone to form defects, which can be explained by the fact that longer tows store more energy and buckle more easily when compressed. In addition, the narrower the tow, the smaller the critical radius and the less prone to buckling. It is obvious that the width has a significant impact on the buckling of the tow, and the small width prepreg can be applicable for automated placement in the trajectory with large curvature.

The increment of the thickness has an obvious inhibitory effect on wrinkle formation. As the thickness of the tow increases, the critical trajectory radius decreases, demonstrating that it is less prone to buckling. Simultaneously, as shown in Figure 4b, the width also plays an important role in the sensitivity of the critical radius to thickness, similar to the role in the influence of the length. More precisely, the positive increase in width reduces the ability of the tow to resist buckling, making it more susceptible to instability in spatial steering.

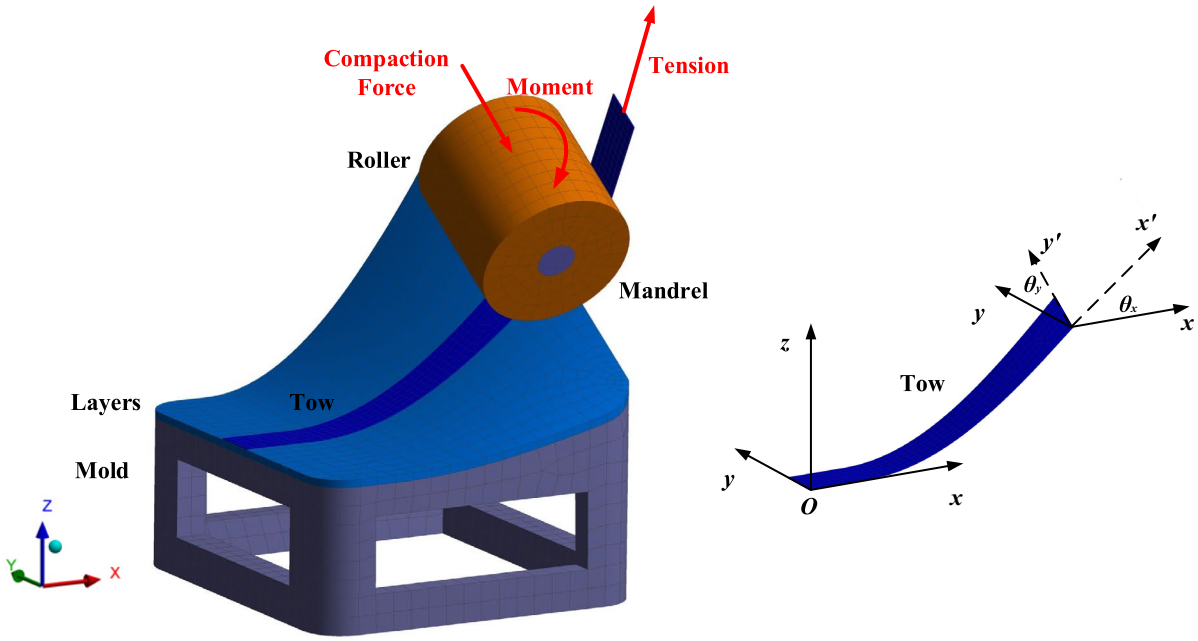

Figure 6 Schematic of tow steering simulation model

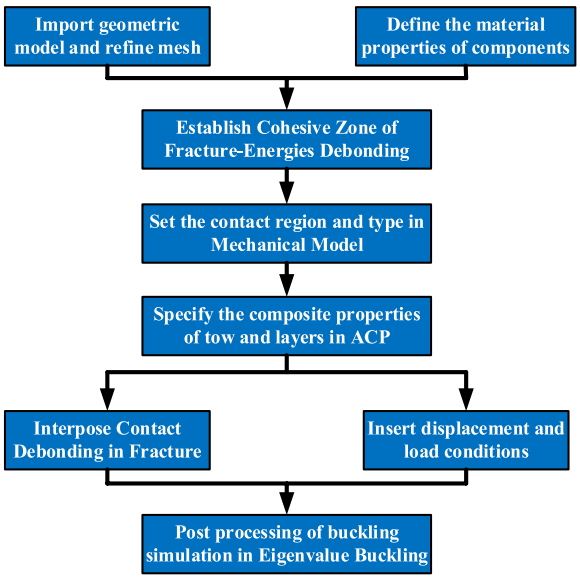

Figure 7 Flow chart of tow steering simulation

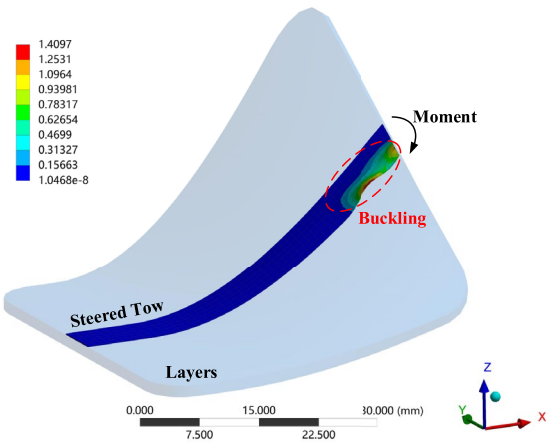

Figure 8 Simulation results of tow buckling

Specifically, when the width of the tow reaches 25.4 mm, a slight increase in thickness allows the tow to withstand a significant increase in trajectory curvature without buckling.

3.1.2 Effect of the Adhesion Coefficient

The adhesion performance between the tow and the mold also has a certain impact on the critical buckling radius. Figure 5 shows the ability of tows with different widths to resist buckling for various adhesion coefficients, in which the larger the adhesion coefficient, the smaller the bending radius of the tow when wrinkling occurs, and the trend of the width influence remains unchanged.

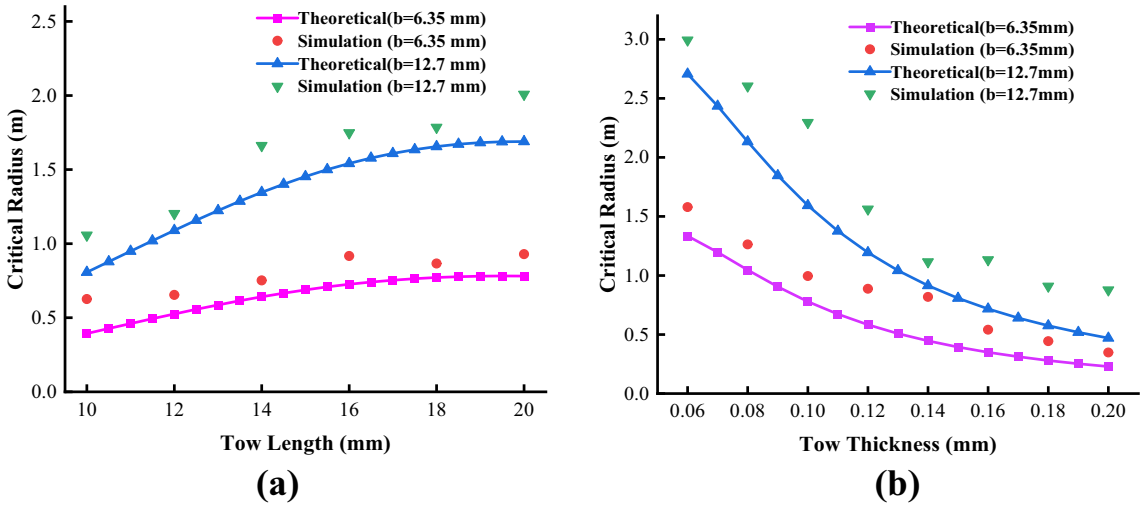

Figure 9 Simulation verification on prepreg parameters: **a** Verification on the influence of tow length, and (**b**) Verification on the influence of tow thickness

3.2 Simulation Modeling Strategy

The simulation model is established by ANSYS software and consists of four important parts: a flexible compaction roller with a rigid mandrel, a prepreg tow to be laid, a mold with a complex surface, and a laminate with a set of layers placed on the mold. The rigid mold can be designed to realize the torsion and warpage of the trajectory corresponding to the rotation of the tow around the coordinate axes in the theoretical model. Additionally, a tensile force is applied at the end of the tow to keep it in tension, and the mandrel is subjected to the compaction force perpendicular to the mold surface and rotates around the vertical axis, so that the tow can be steered in space by the roller. The complete finite element simulation model, external load and rotation conditions of the prepreg tow are shown in Figure 6.

In order to make the model closer to the actual working conditions on the basis of simplified calculation, the contact type between components needs to be optimized. Among them, the contact between the mandrel and the roller, the roller and the tow, the layers and the mold are set as bonded contact, meaning that there is no relative sliding between them, while the contact between the tow to be laid and the laid-up layers is difficult to define due to its role in characterizing the interlayer adhesion. The Cohesive Zone Modeling of ANSYS can be utilized to simulate the delamination mechanism of prepreg in placement process, and the detailed modeling steps are elaborated systematically below.

3.2.1 Modeling Procedure

First, the cohesive zone is established in the engineering data as the interface between the tow and layers to simulate the adhesion performance. The interfacial adhesion is characterized by the fracture-energies based debonding property, of which the maximum normal contact stress and the critical fracture energy for normal separation can be employed to represent the debonding property of the interface. Secondly, the contact debonding failure and buckling analysis mechanism is established in the simulation model, based on which the loads and constraints are applied to solve the stress and strain. The modeling procedure is given in Figure 7.

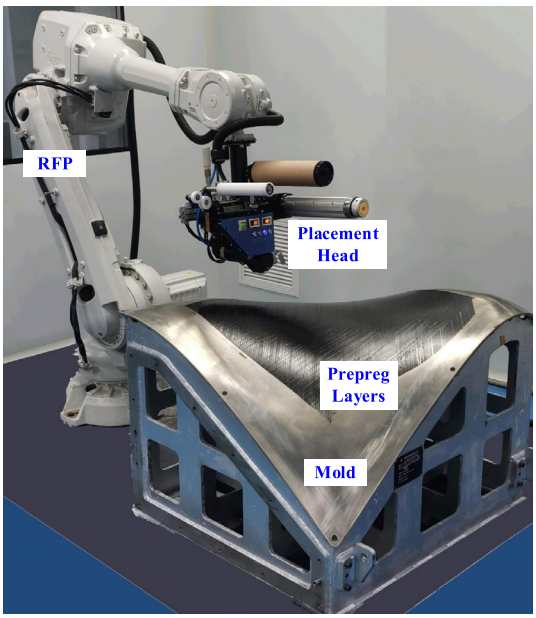

Figure 10 Robotic fiber placement and aerostructure mold

The material of the compaction roller is silicon anisotropic, the prepreg is set as Epoxy Carbon UD prepreg, the mold is structural steel. The buckling phenomenon of the spatial-steered tow is shown in Figure 8. The spatially deformed tow will buckle obviously under the action of in-plane bending moment on the cross-section, resulting in forming defects such as buckling, delamination, and wrinkles.

3.2.2 Simulation Verification

To validate the effect of prepreg dimensions on tow buckling, the critical moments were recorded when the wrinkles appear and the critical radii can be calculated to be compared with theoretical values. In the simulation model, tows with two commonly used widths 6.35 mm and 12.7 mm are adopted for buckling simulation, and the results have been analyzed with the theoretical model.

From Figure 9a, it can be concluded that the simulation results of the dependency of the tow length on the critical radius are generally similar to the theoretical calculation values, especially the trend of the correlation curve is consistent with a theoretical curve in spite of the different widths. The corresponding relationship between the thickness of the tow and the critical radius is shown in Figure 9b, and the trend of the curve is the same as the theoretical calculation results. However, the simulated values of the critical radius in Figure 9 are slightly larger than the theoretical values, indicating that the adhesion in the simulation model has insufficient inhibitory effect on the buckling of the tow. And there is no significant correlation between the difference value and the width, length, and thickness of the tow. The difference is due to minor mismatch in the maximum normal contact stress, critical fracture energy, and adhesion coefficient in the CZM, resulting in insufficient adhesion of the cohesive layer to the tow and mold. This mismatch can be compensated for by correcting the coefficients of CZM to ensure that the curvature of the stress-displacement curve for the simulated detachment of the tow is consistent with the adhesion coefficient *k*. Therefore, despite certain differences, the correspondence between the critical radius and the dimensions of the tow has been verified through simulation models.

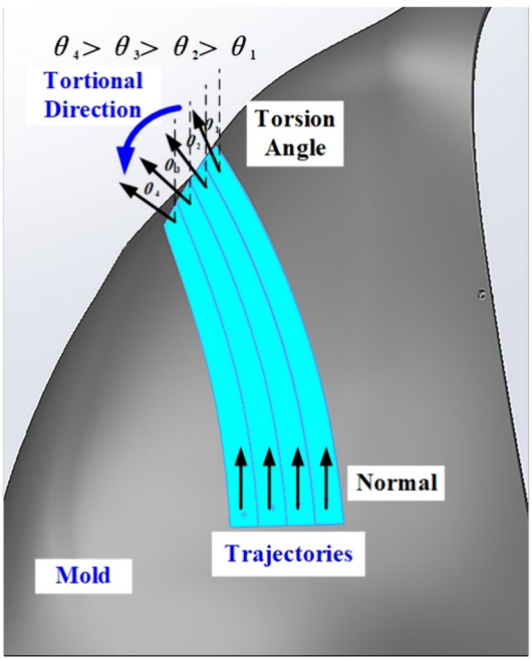

Figure 11 Illustration of torsion state of tows

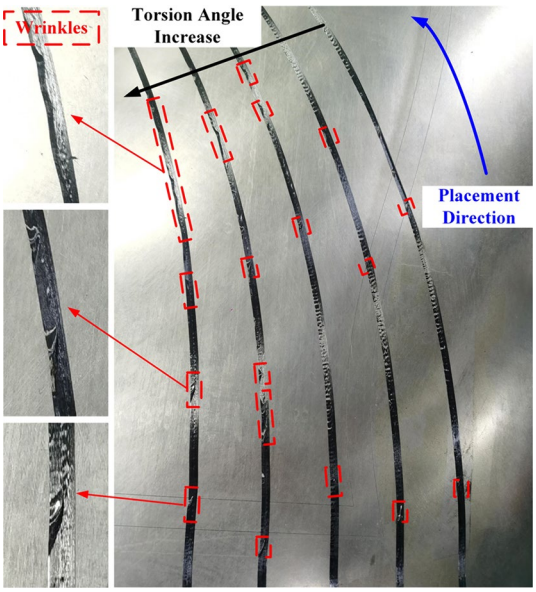

Figure 12 Experimental results for different torsion angles

4 Experimentation and Discussion

The self-developed monofilament robotic fiber placement (RFP) and aerostructure mold shown in Figure 10 were employed for experiments to verify the theory of buckling formation during spatial steering placement. The T700/epoxy prepreg produced by Guangwei Co., Ltd. in Weihai, China, was used for trials, of which the width is 6.35 mm, the tensile strength is 2300 MPa, and the tensile modulus is 115 GPa. The ambient temperature in the laboratory was 21 ℃ and the relative humidity was 28.9%. The resin content of the prepreg is 33%, which shall be stored in the refrigerator for thermal insulation before placement tests. The adjustment of the compaction force can be realized by driving the fiber placement

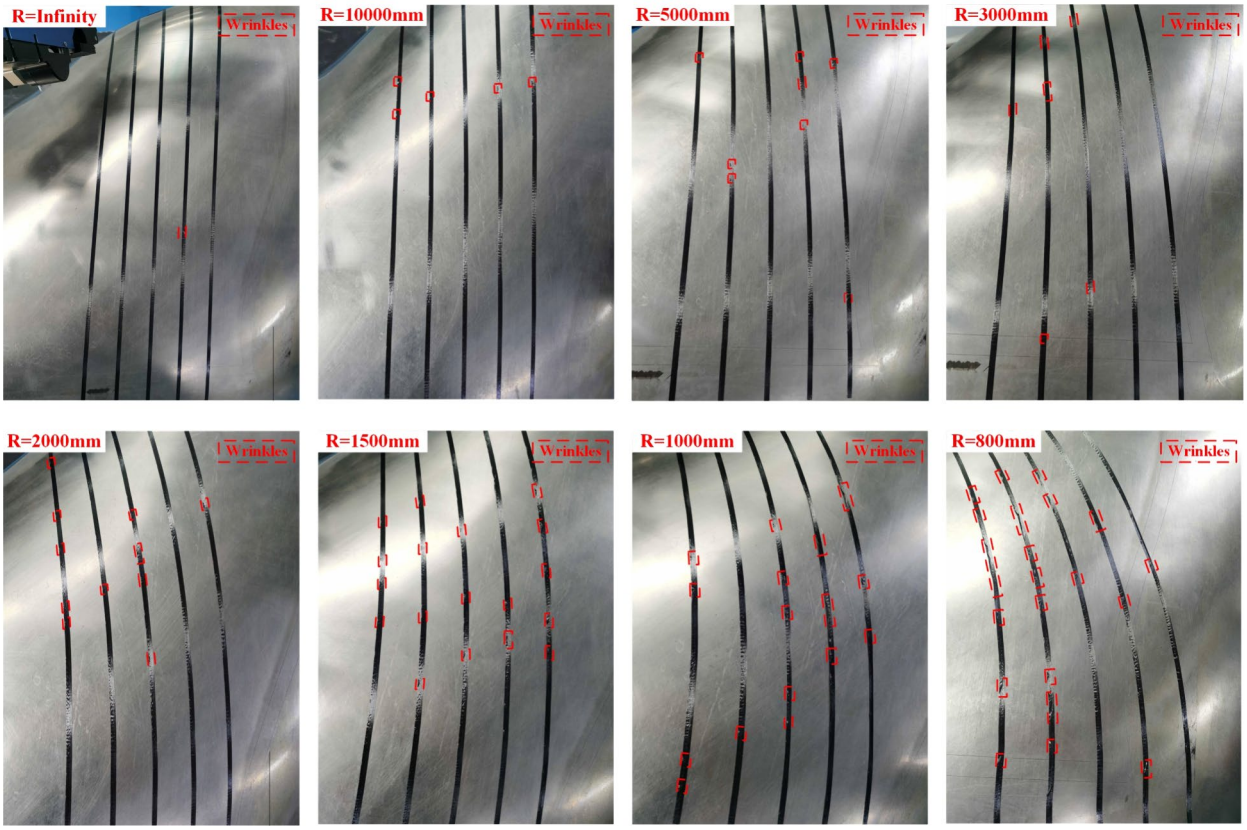

Figure 13 Experimental results for different bending moments

head of the industrial robot to exert pressure on the tows, and the force was monitored in real time by the force sensor installed between the head and the manipulator arm. The temperature of the placement area was set at 40 ℃, heated by infrared heaters mounted in front of the roller on the placement head. The laying velocity was determined by the terminal execution speed of the industrial robot, which can be modified in the motion control program after the completion of the spatial-steering trajectory planning.

4.1 Effect of Torsion Angle

The complex aerostructure mold used in this paper generates multiple trajectories with different torsion angles during placement based on geometric features and mechanical properties. In Figure 11, the prepreg tows are gradually twisted along the placement direction, and the torsion angle increased along the direction of the red arrow. The compaction force was 60 N, the laying-up velocity was 200 mm/s, and the radius of the trajectories was 800 mm.

With the increment of torsion angle, the possibility of buckling increases when the tow is laid along the spatial curved trajectory, and the degree of wrinkles increases significantly as shown in Figure 12. Under the same degree of lateral bending, the tow tends to buckle and form wrinkles at the inner edge, which can be attributed to the increase in potential energy caused by spatial deformation. The greater the torsion, the more wrinkles will be generated, and the leftmost tow with the largest torsion angle has continuous distribution of wrinkles, resulting in a long warped edge.

4.2 Effect of Bending Moment

According to Eq. (22), the smaller the transverse bending radius of the tow, the greater the bending moment in the cross-section. Multiple sets of prepreg tows with different bending moments were laid on the mold, resulting in wrinkles and other defects as shown in Figure 13. The trajectories were straight lines and curves with radii of 10000 mm, 5000 mm, 3000 mm, 2000 mm, 1500 mm, 1000 mm and 800 mm, corresponding to different bending moments. After each group of tows was laid, forming defects were observed and counted, and then removed. Ensure that the temperature of the mold meets the process requirement, and that the groups of different

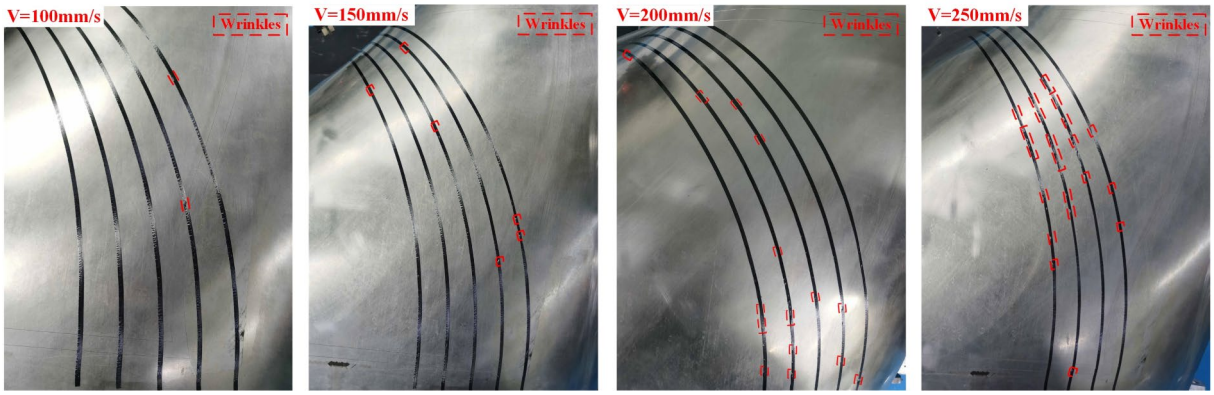

Figure 14 Experimental results for different velocities

trajectories were laid in sequence with the compaction force of 60 N and the velocity of 200 mm/s. It is obvious that as the trajectory radius decreases, the bending moment increases, the number of defects increases, and the laying quality deteriorates, which is highly consistent with the simulation results.

4.3 Effect of Laying-up Velocity

In order to explore the methods for inhibiting the formation of defects in spatial tow steering, verification experiments were conducted respecting the influence of different process parameters on the forming quality. The laying trajectory was a curve with a radius of 800 mm, and the compaction force was 60 N. The variable for this group was the laying velocity, which was 100 mm/s, 150 mm/s, 200 mm/s and 250 mm/s, respectively.

According to the experimental phenomenon shown in Figure 14, the faster the laying velocity, the more forming defects there are. Under the same conditions of compaction force, heating temperature, and other process parameters, the faster the laying velocity, the shorter the compaction time of the roller on the tow, and the poorer the compaction quality. Besides, shorter compaction time leads to a poorer heating effect and also reduces interlayer adhesion performance. According to the adhesion coefficient expression Eq. (28), the increase of velocity means a decrease in adhesion performance, resulting in a worse inhibitory effect of interlayer adhesion on the buckling of the tow, which is not conducive to the suppression of wrinkles.

4.4 Effect of compaction force

In addition, the compaction force also has a significant impact on the placement quality. The force was set to 40 N, 60 N, 80 N, and 100 N, respectively, with a velocity of 200 mm/s. All the trajectories were planned as a curve with the radius of 800 mm on the mold, and the temperature of the placement area was maintained at 40 ℃ throughout the entire laying process.

The degree of defects varied significantly under different force conditions, and sufficient force can effectively suppress the formation of buckling and wrinkles, improving the forming quality, as shown in Figure 15. The effect of compaction force on the adhesion coefficient has been elaborated clearly in Eq. (28), and the force can be appropriately increased to reduce the formation of defects. One of the reasons is that sufficient compaction force can promote the flow of resin between layers, forming an interlayer adhesive layer. Another reason is that the compaction force can increase the deformation degree of the roller, increase the compaction width, extend the compaction time, and improve the compaction quality. However, excessive compaction pressure may lead to uneven resin distribution and tow damage, and an appropriate process window of compaction force needs further experimental exploration.

5 Conclusions

(1) A theoretical model based on the first-order shear deformation theory, Hertz contact and intimate contact theory is established to reveal the defects formation mechanism in spatial tow steering for complex structure placement forming, and the governing equation is solved by the improved deflection equation involving the elastic bonding interface, the spatial rotation angle function and the principle of minimum potential energy to obtain the critical load for tow buckling.

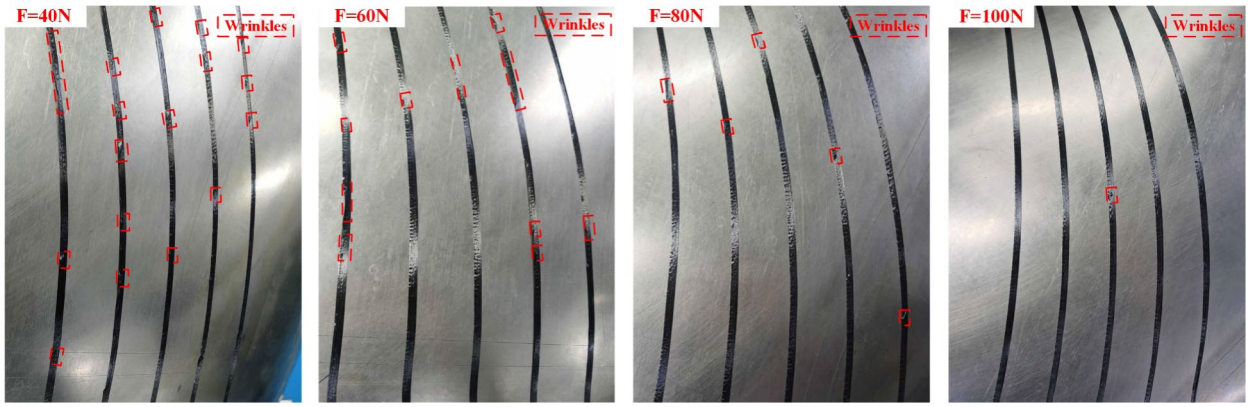

Figure 15 Experimental results for different compaction forces

(2) The CZM-based modeling method is proposed to simulate the interlayer adhesion and the formation of wrinkles on the inner edge of the tow, and the sensitivity analysis shows that the dimensions of the prepreg and the interfacial adhesion coefficient have a significant impact on the critical radius of the spatial steered tow.

(3) A series of experiments for spatial steering placement are conducted to reveal the influence of torsion angle, in-plane bending moment, laying-up velocity and compaction force on tow buckling, and the effectiveness of optimizing process parameters in suppressing the formation of defects is verified through single-factor test.

Author contributions

MY and FL were in charge of the whole trial; MY wrote the manuscript; BC and YZ conducted the experiments; XD and WZ assisted with the research ides and structure of the manuscript. All authors read and approved the final manuscript.

Funding

Supported by National Natural Science Foundation of China (Grant Nos. 52205003 and 51575018), Zhejiang Provincial Natural Science Foundation (Grant No. LD22E050011) and Ningbo Municipal Key Projects of Science and Technology Innovation 2025 Plan (Grant No. 2022Z070).

Data availability

The data are available from the corresponding author on reasonable request.

Declarations

Competing interests

The authors declare no competing financial interests.

Received: 23 November 2023 Revised: 9 July 2024 Accepted: 22 July 2024
Published online: 22 August 2024

References

[1] Alex Brasington, Christopher Sacco, Joshua Halbritter, et al. Automated fiber placement: A review of history, current technologies, and future paths forward. *Composites Part C: Open Access*, 2021, 6(3): 98-115.

[2] Ebrahim Oromiehie, B. Gangadhara Prusty, Paul Compston, et al. Automated fibre placement based composite structures: Review on the defects, impacts and inspections techniques. *Composite Structures*, 2019, 224(18): 109-122.

[3] Wuxiang Zhang, Fei Liu, Yongxin Lv, et al. Design and analysis of a metamorphic mechanism for automated fibre placement. *Mechanism and Machine Theory*, 2018, 130(12): 463-476.

[4] Wuxiang Zhang, Fei Liu, Tao Jiang, et al. Overview of current design and analysis of potential theories for automated fibre placement mechanisms. *Chinese Journal of Aeronautics*, 2022, 35(4): 1-13.

[5] Stephen Barr, Justin Jaworski. Optimization of tow-steered composite wind turbine blades for static aeroelastic performance. *Renewable Energy*, 2019, 139(10): 859-872.

[6] Bret Stanford, Christine Jutte. Comparison of curvilinear stiffeners and tow steered composites for aeroelastic tailoring of aircraft wings. *Computers and Structures*, 2017, 183(6): 48-60.

[7] Isabel Martin, Diego Saenz Del Castillo, Antonio Fernandez, et al. Advanced thermoplastic composite manufacturing by in-situ consolidation: A review. *Journal of Composites Science*, 2020, 4(4): 745-780.

[8] Byung Chul Kim, Paul M. Weaver, Kevin Potter. Computer aided modelling of variable angle tow composites manufactured by continuous tow shearing. *Composite Structures*, 2015, 129(11): 256-267.

[9] Byung Chul Kim, Kevin Potter, Paul Weaver. Continuous tow shearing for manufacturing variable angle tow composites. *Composites Part A: Applied Science and Manufacturing*, 2012, 43(8): 1347-1356.

[10] Phyo Thu Maung, Gangadhara Prusty, Andrew Phillips, et al. Curved fibre path optimisation for improved shape adaptive composite propeller blade design. *Composite Structures*, 2021, 255(1): 610-622.

[11] Dirk Lukaszewicz, Carwyn Ward, Kevin Potter. The engineering aspects of automated prepreg layup: History, present and future. *Composites Part B: Engineering*, 2012, 43(3): 997-1009.

[12] Devesh Punera, Paulomi Mukherjee. Recent developments in manufacturing, mechanics, and design optimization of variable stiffness composites. *Journal of Reinforced Plastics and Composites*, 2022, 41(23): 917 - 945.

[13] Alexis Beakou, Le Cam, Vincent Verney. Modelling slit tape buckling during automated prepreg manufacturing: A local approach. *Composite Structures*, 2011, 93(10): 2628-2635.

[14] Xiaodong Chen, Guojun Nie, Zhangming Wu. Application of Rayleigh-Ritz formulation to thermomechanical buckling of variable angle tow composite plates with general in-plane boundary constraint. *International Journal of Mechanical Sciences*, 2020, 187(23): 375-396.

[15] Mikhail Matveev, Peter Schubel, Andrew Long, et al. Understanding the buckling behaviour of steered tows in automated dry fibre placement (ADFP). *Composites Part A: Applied Science and Manufacturing*, 2016, 90(11): 451-456.
[16] Meisam Kheradpishe, Mehdi Hojjati. Wrinkle formation and initial defect sensitivity of steered tow in automated fiber placement. *Journal of Composites Science*, 2021, 5(11): 191-205.
[17] Muhsan Belhaj, Mehdi Hojjati. Wrinkle formation during steering in automated fiber placement: Modeling and experimental verification. *Journal of Reinforced Plastics and Composites*, 2018, 37(6): 396-409.
[18] Nima Bakhshi, Mehdi Hojjati. Time-dependent wrinkle formation during tow steering in automated fiber placement. *Composites Part B: Engineering*, 2019, 165(10): 586-593.
[19] Yi Wang, Sarthak Mahapatra, Jonathan Belnoue, et al. Modelling the effect of process conditions on steering-induced defects in automated fibre placement (AFP). *Composites Part A: Applied Science and Manufacturing*, 2023, 173(10): 783-797.
[20] Gangadharan Raju, Zhangming Wu, Byung Chul Kim, et al. Prebuckling and buckling analysis of variable angle tow plates with general boundary conditions. *Composite Structures*, 2012, 94(9): 2961-2970.
[21] Helin Pan, Di Yang, Weiwei Qu, et al. Process-dependent wrinkle formation for steered tow during automated fiber placement: Modeling and experimental verification. *Thin-Walled Structures*, 2022, 180(11): 1083-1094.
[22] Minh Hoang Nguyen, Avinkrishnan Vijayachandran, Paul Davidson, et al. Effect of automated fiber placement (AFP) manufacturing signature on mechanical performance of composite structure. *Composite Structures*, 2019, 228(22): 191-219.
[23] Minghui Yi, Fei Liu, Wuxiang Zhang, et al. Formation mechanism and modeling method of wrinkling defects in variable angle tow steering fiber placement. *Aerospace*, 2022, 9(10): 190-215.
[24] Ozan Çelik, Daniël Peeters, Clemens Dransfeld, et al. Intimate contact development during laser assisted fiber placement: Microstructure and effect of process parameters. *Composites Part A: Applied Science and Manufacturing*, 2020, 134(7): 55-67.
[25] Junxia Jiang, Yuxiao He, Han Wang, et al. Modeling and experimental validation of compaction pressure distribution for automated fiber placement *Composite Structures*, 2021, 256(2): 883-892.
[26] Jinxiang Cheng, Dongbiao Zhao, Kai Liu, et al. Modeling and impact analysis on contact characteristic of the compaction roller for composite automated placement. *Journal of Reinforced Plastics and Composites*, 2018, 37(23): 1418-1432.
[27] Sreehari Rajan, Michael A. Sutton, Roudy Wehbe, et al. Experimental investigation of prepreg slit tape wrinkling during automated fiber placement process using StereoDIC. *Composites Part B: Engineering*, 2019, 160(5): 546-557.
[28] Pan Zhao, Bijan Shirinzadeh, Yaoyao Shi, et al. Multi-pass layup process for thermoplastic composites using robotic fiber placement. *Robotics and Computer Integrated Manufacturing*, 2018, 49(1): 277-284.
[29] Dennis Budelmann, Carsten Schmidt, Leif Steuernagel, et al. Adhesion-cohesion balance of prepreg tack in thermoset automated fiber placement. *Composites Part C: Open Access*, 2023, 12(3): 181-194.
[30] Muhsan Belhaj, Ali Dodangeh, Mehdi Hojjati. Experimental investigation of prepreg tackiness in automated fiber placement. *Composite Structures*, 2021, 262(8): 51-63.
[31] Roudy Wehbe, Brian Tatting, Sreehari Rajan, et al. Geometrical modeling of tow wrinkles in automated fiber placement. *Composite Structures*, 2020, 246(16): 166-179.
[32] Byung Chul Kim, Paul Weaver, Kevin Potter. Manufacturing characteristics of the continuous tow shearing method for manufacturing of variable angle tow composites. *Composites Part A: Applied Science and Manufacturing*, 2014, 61(6): 141-151.
[33] Junxia Jiang, Yuxiao He, Yinglin Ke. Pressure distribution for automated fiber placement and design optimization of compaction rollers. *Journal of Reinforced Plastics and Composites*, 2019, 38(18): 860-870.
[34] Nima Bakhshi, Mehdi Hojjati. An experimental and simulative study on the defects appeared during tow steering in automated fiber placement. *Composites Part A: Applied Science and Manufacturing*, 2018, 113(10): 122-131.
[35] Yi Di Boon, Sunil Chandrakant Joshi, Somen Kumar Bhudolia. Review: Filament winding and automated fiber placement with in situ consolidation for fiber reinforced thermoplastic polymer composites. *Polymers*, 2021, 13(12): 1498-1526.
[36] Matthew Donough, Shafaq, Nigel John, et al. Process modelling of in-situ consolidated thermoplastic composite by automated fibre placement-A review. *Composites Part A: Applied Science and Manufacturing*, 2022, 163(12): 26-47.
[37] Nima Bakhsh, Mehdi Hojjati. Effect of compaction roller on layup quality and defects formation in automated fiber placement. *Journal of Reinforced Plastics and Composites*, 2019, 39(2): 3-20.

Minghui Yi born in 1994, is currently a PhD candidate at *School of Mechanical Engineering and Automation, Beihang University, China*. His research interests include the process regulation and equipment development for automated fiber placement.

Fei Liu born in 1992, is currently a postdoctoral researcher at *School of Mechanical Engineering and Automation, Beihang University, China*. She received her PhD degree from *Beihang University, China*, in 2022. Her research interests include mechanism design and layout optimization of composite structure forming equipment.

Baoning Chang is currently an associate research fellow at *Advanced Manufacturing Center, Ningbo Institute of Technology, Beihang University, China*. He received his PhD degree from *Dalian University of Technology, China*, in 2020. His research interests include mechanics of composite materials and equipment design.

Yingdan Zhu is currently senior researcher at *Ningbo Institute of Materials, CAS, China*. She received her PhD degree from *Wuhan University of Technology, China*, in 2005. Her research interests include intelligent manufacturing and equipment of composite materials.

Xilun Ding born in 1967, is currently a professor at *School of Mechanical Engineering and Automation, Beihang University, China*. He received his PhD degree from *Harbin Institute of Technology, China*, in 1997. His research interests include the multi-scale optimization design of composite structure and equipment integration.

Wuxiang Zhang born in 1978, is currently a professor at *School of Mechanical Engineering and Automation, Beihang University, China*. He received his PhD degree from *Beihang University, China*, in 2009. His research interests include the optimization design of composite material automation manufacturing equipment.